

Simultaneous optimisation of temperature and energy in linear energy system models

Patrik Schönfeldt, Adrian Grimm, Bhawana Neupane,
Herena Torio, Pedro Duran, Peter Klement, Benedikt Hanke,
Karsten von Maydell, and Carsten Agert

DLR Institute of Networked Energy Systems,
Carl-von-Ossietzky-Str. 15, 26129 Oldenburg, Germany

December 24, 2020

Abstract

Linear programming is used as a standard tool for optimising unit commitment or power flows in energy supply systems. For heat supply systems, however, it faces a relevant limitation: For them, energy yield depends on the output temperature, thus both quantities would have to be optimised simultaneously and the resulting problem is quadratic. As a solution, we describe a method working with discrete temperature levels. This paper presents mathematical models of various technologies and displays their potential in a case study focused on integrated residential heat and electricity supply. It is shown that the technique yields reasonable results including the choice of operational temperatures.

1 Introduction

Space heating accounts for approximately one third of the global final energy consumption in both, the residential and the commercial building sub-sectors. Including hot water, the demand for low temperature heat was 17.4 PWh in 2010, which makes 53% of the total final energy demand of the worldwide building sector [1]. Still in 2019, the share of renewable energy supply only meets 11% of the global heat demand, leading to a domination of fossil fuels in this sector, contributing 40% (13.3 Gt) of global CO₂ emissions [2].

This fact imposes a need for energy system optimisation in the heat sector. As the efficiency of renewable heat sources such as solar thermal plants or heat pumps shows a significant dependency on the temperature, it should be considered in the optimisation. However, while numerical descriptions including both, energy and temperature, are common for pure physical models (i.e. [3, 4, 5]), cross-sectorial optimisation models typically lack according formulations (cf. [6, 7, 8]). A reason is that the commonly used technique of linear programming does not allow straightforward implementations that would require the product of optimisation variables. To tackle this problem, the non-linear problem can be modelled (e.g. [9, 10, 11]), but there are further options:

A possible solution is presented in [12]. These authors subdivide the problem into two parts: The storage is modeled by sub-volumes of constant size, making temperature the optimisation variable. Outside the storage, mass flows are optimised. Alternatively, possible mass flows can be pre-calculated. When deviations from this value are assumed to be small, temperature and heat calculations can be decoupled [13, 14]. When iterating over such a linear model using different possible mass flows, it will eventually converge. An alternative approach works with discrete, fixed values for either the mass flows [15], or the temperature levels [8].

The present work follows the latter approach but introduces modifications to reduce the computational effort. It also extends prior work using discrete temperature levels by allowing for variable temperature levels at all parts of the model. Also, an example study implementing the method using `oemof.solph` [16] is presented. In the study, the operation of a solar based residential energy supply system is optimised either for economical costs or exergy.

2 Mathematical models

The thermal energy of a volume V of matter at temperature T with $[T] = 1 \text{ K}$ is

$$E_{\text{th}}(T, V) = \rho c_p T V, \quad (1)$$

where ρ is the density and c_p is the thermal capacity of the medium. When there is a lower temperature level T_{low} and a higher one T_{high} , it is convenient to also define a heat energy resulting from the temperature difference

$$Q(T_s) := E_{\text{th}}(T_{\text{high}} - T_{\text{low}}). \quad (2)$$

Assuming a pipe diameter d the transferred heat then is

$$\dot{Q} = \rho c_p \dot{V} \times (T_{\text{high}} - T_{\text{low}}) \quad (3a)$$

$$= \rho c_p d v \times (T_{\text{high}} - T_{\text{low}}), \quad (3b)$$

where v marks the velocity of the matter at temperature T_{high} . Having in mind temperature-dependent losses and efficiencies, it makes sense to optimise both, temperature and transferred volume (\dot{V}) simultaneously. However, as they are both factors in the same product, linear programming does not allow to have variables for both at the same time. Thus it is not straightforward to optimise both using this optimisation technique. As a workaround, we introduce k discrete temperature levels with

$$T_{\text{high}} \geq T_{n+1} > T_n \geq T_{\text{low}}, \quad n \in 0 \dots k-1. \quad (4)$$

For these fixed temperature levels, instead of Eq. (3b), it is now possible to optimise

$$\dot{Q} = \sum_{n=0}^{k-1} \rho c_p d \times v_n \times (T_n - T_{\text{low}}), \quad (5)$$

where special conditions might apply for the v_n . For example, if only one temperature level $T_m(t)$ can be active at a time, it would be $v_n(t) = 0 \forall n \neq m(t)$.

In the following, $\dot{Q}_{\text{in},n}$ identifies a heat flow to the level at T_n , while $\dot{Q}_{\text{out},n}$ marks a heat flow from the level T_n to another level at T_m with $n \neq m$.

2.1 Heat sources

We assume that the temperature can always be reduced. Thus, any heat source s supplying heat at T_n can supply at least the same amount of heat at T_{n-1} , hence

$$\dot{Q}_{s,n-1,\max} \geq \dot{Q}_{s,n,\max}. \quad (6)$$

Also, heat is always gradually increased, from one temperature level to the next. The heat entering the heat supply system \dot{Q}_{in} at T_n is composed of the supply coming from the external source at that level $\dot{Q}_s(T_n)$ and heat taken from the lower level $\dot{Q}_{\text{out}}(T_{n-1})$

$$\begin{aligned} \dot{Q}_{\text{in},n} &= (1 - r_{n,n-1}) \times \dot{Q}_{\text{out},n-1} \\ &+ r_{n,n-1} \times \dot{Q}_{s,n}, \end{aligned} \quad (7a)$$

where

$$r_{n,n-1} = \frac{T_n - T_{n-1}}{T_n - T_{\text{low}}}. \quad (7b)$$

This guarantees that heat can not be transferred from a lower to a higher level without applying external work.

2.1.1 Heat sources with constant efficiencies

For heat sources with an efficiency that does not depend on the target temperature, only the highest relevant temperature output $\dot{Q}_s(T_s) = \dot{Q}_{s,k-1}$ has to be modelled. This is the case, e.g for boilers (gas, pellets, oil) or electric heating rods. Equation 6 is then implemented using a possible lossless heat flow from Q_n to Q_{n-1} . In combination with Eq. (7a), this yields

$$\dot{Q}_s = \sum_n \dot{Q}_{\text{in},n}, \quad (8)$$

which is the expected result.

2.1.2 Heat sources with temperature-dependent efficiencies

Especially heat pumps or solar thermal plants – heat sources that play a large role in renewable heat supply – have temperature-dependent efficiencies $\eta_s(T)$. Having predefined temperature levels allows to pre-calculate these for all T_n . This way, a maximum supply is modeled for every possible combination of temperature level and supply technology,

$$\dot{Q}_{s,n} \leq \dot{Q}_{s,n,\max} \quad \forall n > 0. \quad (9)$$

To avoid increased production of heat due to the increased number of sources, binary status variables $s_{s,n} \in 0, 1$ can be added, with¹

$$\sum_n s_{s,n} \leq 1 \quad \forall s \quad (10a)$$

$$\dot{Q}_{s,n} \leq s_{s,n} \times \dot{Q}_{s,n,\max} \quad \forall s, n. \quad (10b)$$

¹Constraint `max_active_flow_count` in `oemof.solph`.

While this approach is realistic, it has to be considered that binary variables may introduce performance issues. So, as an alternative to Eq. (10), partial use at all levels can be allowed by introducing non-exclusive status variables $q_{s,n} \geq 0$ with

$$\sum_n q_{s,n} \leq 1 \quad \forall s \quad (11a)$$

$$q_{s,n} \times \dot{Q}_{s,n,\max} = \dot{Q}_{s,n} \quad \forall s, n. \quad (11b)$$

If storage is in place, this can be justified by the presence of finite time steps in the optimisation: Even if the temperature levels have to be served exclusively at a certain time, the level might be switched within one time step.

2.2 Heat storage

Analogue to [8], the total storage volume is split up into k sub-volumes to map the temperature levels. These form a stepped temperature-distribution model [5, Sec. 4.2.]

$$V = \sum_{n=0}^{k-1} V_n(t) \quad (12)$$

each with a homogeneous temperature T_n that is chosen to be constant in time. To reduce complexity, we exclude temperature inversion. This is already implied by Eq. (4). Further, we assume the tank to be cylindrical. Thus the volume is

$$V_n(t) = h_n(t) \times \pi r^2 \quad (13)$$

and the surfaces are

$$A_n = \begin{cases} 2\pi r h_n & 0 < n < k-1 \\ 2\pi r h_n + \pi r^2 & n = 0 \vee n = k-1, \end{cases} \quad (14a)$$

$$(14b)$$

Although $\sum \dot{V}_n = 0$, by setting the lowest temperature level $T_0 = T_i$, losses do not mean a heat exchange in the sense of $\dot{Q}_n > 0$, as for losses

$$\dot{V}_n \leq 0 \quad \forall n > 1 \quad (15a)$$

and due to the choice of T_0

$$Q(V_0) \equiv 0. \quad (15b)$$

When setting $T_0 = T_i$ to the ambient temperature T_A , the heat loss is

$$\dot{Q}_n = (T_n - T_A) \times \dot{V}_n \rho c_p \quad (16a)$$

$$= -\frac{\lambda}{d_{\text{iso}}} (T_n - T_A) \times A_n(t). \quad (16b)$$

Using Eq. (14), $h_{n,0} = h_n(t=0)$ we get

$$h_n(t) = \begin{cases} h_{n,0} \times e^{-t/\tau_{\text{MB}}} & 0 < n < k-1 \\ h_{n,0} \times e^{-t/\tau_{\text{MB}}} + \pi \frac{r}{2} & n = k-1 \end{cases} \quad (17a)$$

$$(17b)$$

where the second term accounts for losses at the top side. As the sub-volumes are independent, they might be implemented as one individual storage for each temperature level [17], as long as Eq. (12) is preserved by neglecting the n surfaces $A_{0,n}$ of the lowest level, which is now present multiple times.

If the ambient temperature $T_A(t)$ is variable, the stored heat according to Eq. (2) can change, even if nothing changes in the storage. To account for this, virtual heat flows

$$\dot{Q}_{A,n} = -\dot{T}V_n\rho c_p \quad (18)$$

have to be added for all sub-volumes V_n with $n > 0$ that modify the stored energy accordingly. Alternatively, a constant $T_0 \approx T_A(t)$ can be chosen, if the losses for $n = 0$ remain small compared to those at T_n with $n > 0$. This argument remains true if a representation based on multiple individual storage tanks for the temperature levels is picked. However, the influence of the 0th step on the losses will be overestimated as there is an $A_{n,0} \forall n > 0$. In total

$$\sum_{n=1}^k (A_{n,0}) = (k-1) \times A - \sum_{n=1}^k A_n \quad (19a)$$

$$= (k-2) \times A + A_0, \quad (19b)$$

meaning the surface of the 0th level is overestimated by an offset proportional to the total surface of the storage.

Comparing our approach with the one of [8], there are some significant differences: While we model losses as virtual heat flows directly to the lowest level, they connect adjacent sub-volumes [18]. While the latter is more realistic, our approach allows for dropping the binary variable that indicates whether or not a temperature level is active. This fact alone typically comes with an advantage in computational performance [19, 20]. Also, it is the key to further simplify the formulation by allowing alternative representation using $k-1$ storage tanks with just two layers, each.

2.3 Heat demands

Heat demands \dot{Q}_d are modeled by a reduction of the temperature, regardless if that reduction really happens or if fresh, cold water is replacing hot water in the tank (i.e. when showering). Analogue to Eq. (7a), we have

$$\begin{aligned} \dot{Q}_{\text{out},n} &= r_{n,m} \times \dot{Q}_{d,n} \\ &+ (1 - r_{n,m}) \times \dot{Q}_{\text{in},m}, \end{aligned} \quad (20a)$$

where

$$r_{n,m} = \frac{T_n - T_m}{T_n - T_{\text{low}}}. \quad (20b)$$

So, just in the special case of $T_m = T_{\text{low}}$ all heat taken at level T_n fulfills the demand at that level. Typically it partly increases the heat at the level $T_m < T_n$.

3 Case study

3.1 Energy system layout

As an example, we optimise the control strategy of an integrated energy supply system of a residential block using the presented techniques. The parameters have been chosen to be realistic for the quarter “Helleheide” [21] located in north-western Germany, which is being developed in the framework of the research project “Energetisches Nachbarschaftsquartier Fliegerhorst Oldenburg” (short ENaQ). The used energy system model consists of a number of energy supply and conversion technologies as well as two heat storage tanks. A graph representing this energy system is depicted in Fig. 1.

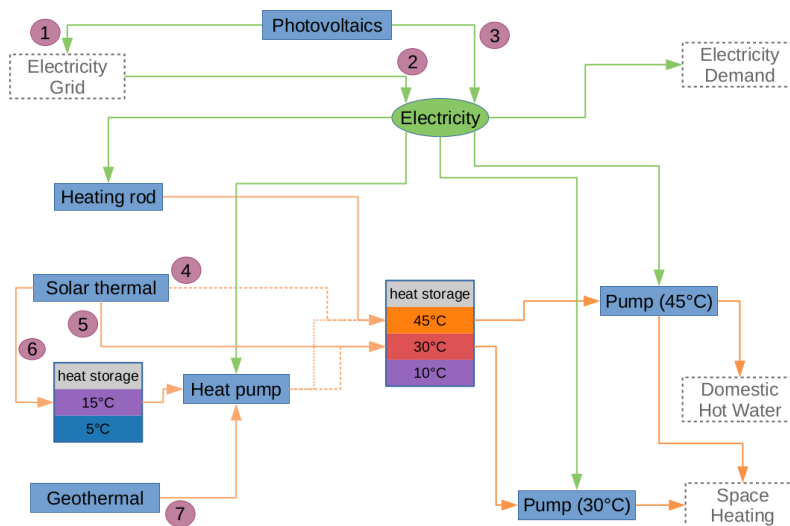


Figure 1: Energy system graph of example scenario. Lines signify possible energy flows between components, dashed or dotted lines have no special meaning, the individual styles just makes them distinguishable. The numbers mark energy flows that have an attached cost (see Tab. 1).

We assume about 140 residential units, resulting in a demand for electricity of $E_{el} = 376 \text{ MWh/a}$ and heat demands of $Q_{SH} = 402 \text{ MWh/a}$ at at least 30°C for space heating and $Q_{DHW} = 336 \text{ MWh/a}$ at 45°C for domestic hot water. Besides economical costs (in EUR), we optimise for an exergy rating $X(T_A(t))$ that varies with the ambient temperature. Electrical power to pump the heat to the demand is assumed to be 1% of the transported heat for the higher and 2% of the transported heat for the lower temperature level.

On the supply side, there are a PV power plant ($P_{peak} = 150 \text{ kW}$), solar thermal collectors ($A = 1050 \text{ m}^2$), and a geothermal collector ($P_{th,max} = 100 \text{ kW}, T = T_{soil}(t)$). All three show weather dependent characteristics. The solar thermal collector is implemented using the technique described in Sec. 2.1.2, so it reflects the trade-of between energy gain and achievable temperature. The

same is true for the heat pump ($P_{\text{th}} = 280 \text{ kW}$), which can be used to raise the temperature from either $T_{\text{soil}}(t)$ or $15 \text{ }^\circ\text{C}$ to either $30 \text{ }^\circ\text{C}$ or $45 \text{ }^\circ\text{C}$. For this, coefficients of performance (COPs) of 30 % of the Carnot COP $1/\eta_c$, see Eq. (21), are considered.

Further, there are a cold and a warm heat storage ($V = 50 \text{ m}^3$ each). These are modeled according to Sec. 2.2. The cold storage solely serves as a source for the heat pump and uses $T_0 = 5 \text{ }^\circ\text{C}$. The warm storage is used to fulfill the demands and has $T_0 = 10 \text{ }^\circ\text{C}$, which is considered the temperature of fresh water. Both storage tanks can get energy from the solar thermal collector. Additionally, the warm storage is fed by the heat pump or an electric heating rod $\eta = 95 \%$ serving as a backup. Note that the energy system layout has been chosen to see the applicability and plausibility of the method on a realistic heat energy supply system. It does not necessarily represent an energy system of optimal performance though.

3.2 Input data

no.	Prices (EUR/MWh)	Exergy (MWh/MWh)
1	-72.90	0
2	34.07 ... 280.65	1.224 ... 1.704
3	67.56	1.0
4	0	0.000 ... 0.080
5	0	0.000 ... 0.126
6	0	0.047 ... 0.167
7	0	0.000 ... 0.057

Table 1: Costs in optimisation of the model (Fig. 1). The dots signify a range in which the value varies within the year 2017, which was taken as an example in the study.

Input data consists of hourly time series for prices, weather, and grid electricity for the year 2017. An overview is given in Tab. 1. Further, there are demand time series with the same resolution. The time series for space heating has been prepared according to [22] using **QuaSi** [23], the ones for electricity and domestic hot water using the **Load Profile Generator** [24].

The applicable prices include (see [25, p. 41] for details)

1. funding for pv feed in to the grid
2. the day ahead price [26] plus all applicable taxes and levies, and
3. renewable energy levy according to German EEG.

Figure 2 shows the variations over the year and a price-duration curve.

The exergy of electricity from the grid is based on [22]. There, the emissions from electricity in the grid are calculated as an hour-specific average and dependent on the power plants operating in a particular region within the European transmission grid. In the same way, we calculate the share of fossil and renewable energy feed-ins for each hour in 2017, based on data of the entso-e [26] for

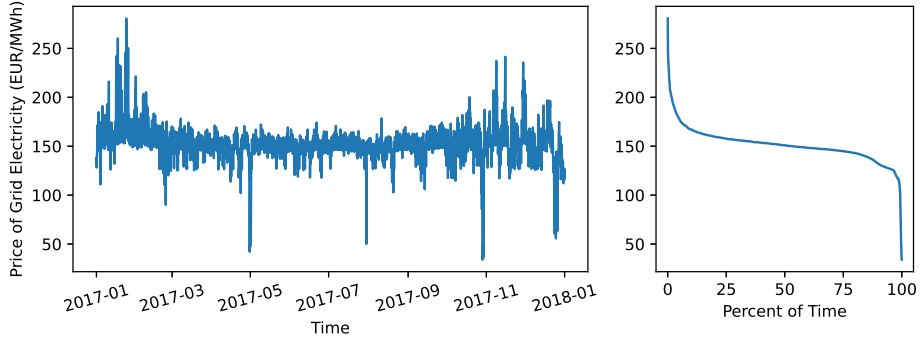


Figure 2: hour-specific costs for imports of electricity in terms of prices over time for two exemplary weeks of the year

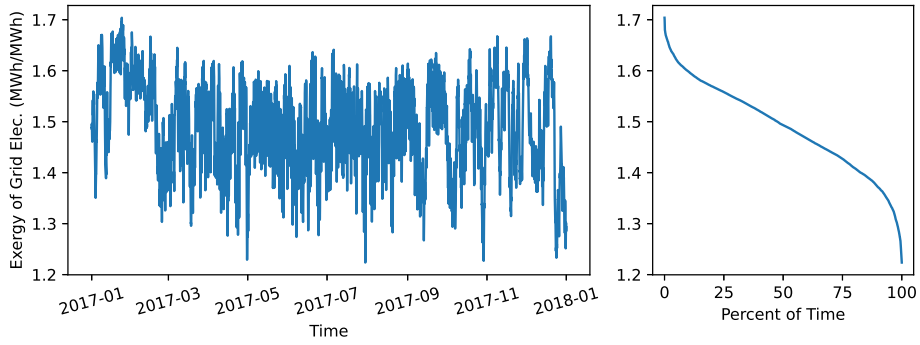


Figure 3: hour-specific costs for imports of electricity in terms of relative exergy-input over time for two exemplary weeks of the year

the region *DE-AT-LU*. For fossil-based energy, we assume 1.8 MWh/MWh , which is the primary energy factors of the power plants according to [27], as a best available guess for the relative exergy-input. For renewable-based grid electricity, we set 1.05 MWh/MWh , considering a 5% loss in the grid, local PV electricity has a value of 1.0 MWh/MWh . The combination of these data leads to the minimum and maximum value for the exergy of the electricity from the grid shown in Table 1, The values over the year and a duration curve are displayed in Fig. 3. As the temperatures are assumed to be constant, the other exergy ratings are calculated using the Carnot efficiency

$$\eta_c = 1 - \frac{T_{\text{low}}}{T_{\text{high}}}, \quad (21)$$

where T_{low} and T_{high} are the minimum and the maximum of the air temperature the temperature valid for the technology, respectively. So, the weights are

4. $\eta_{15}(t) = 1 - \min(288.15 \text{ K}, T_A) / \max(288.15 \text{ K}, T_A)$
5. $\eta_{30}(t) = 1 - \min(303.15 \text{ K}, T_A) / \max(303.15 \text{ K}, T_A)$
6. $\eta_{45}(t) = 1 - \min(318.15 \text{ K}, T_A) / \max(318.15 \text{ K}, T_A)$

Quantity	Unit	Price-optimal	Exergy-optimal
Operational costs	EUR/MWh	53.68	54.16
Exergy per Energy	MWh/MWh	0.617	0.611
Specific emissions	kg/MWh	168	167
Solar heat (15 °C)	MWh/a	25.7	27.6
Solar heat (30 °C)	MWh/a	14.9	75.1
Solar heat (45 °C)	MWh/a	270	210
Pumping electricity	MWh/a	10.6	11.1

Table 2: Resulting values for both optimisation cases.

$$7. \eta_{\text{soil}}(t) = 1 - \min(T_{\text{soil}}, T_A) / \max(T_{\text{soil}}, T_A)$$

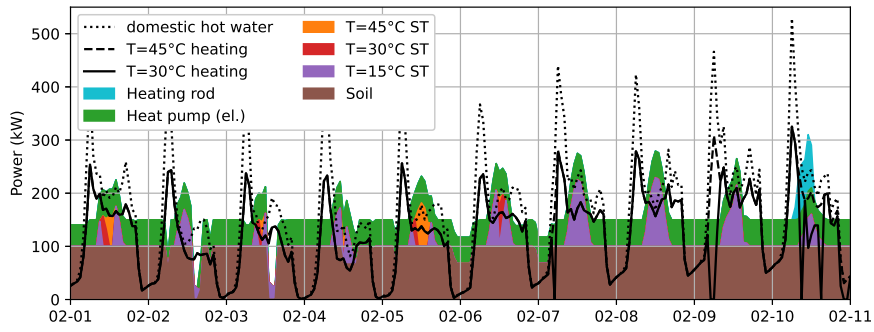
for the corresponding energy flows.

3.3 Optimisation results

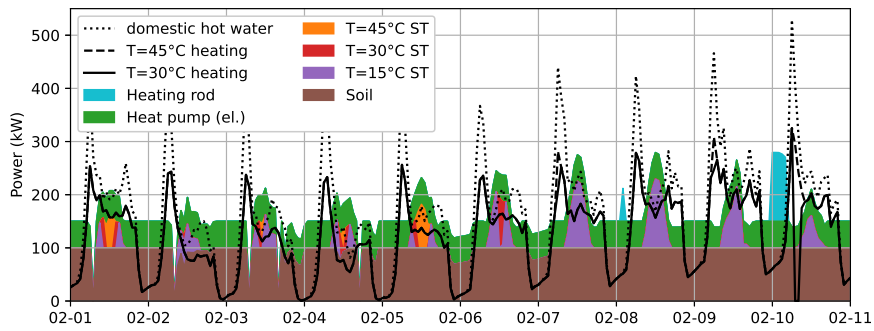
The optimisation is run for the whole year 2017, for both, prices and exergy. For the first ten days of February, the heat energy balance (heat being produced and used) and the storage content (in relative volume) are displayed in Fig. 4. The values for the variables are displayed in Table 2.

In Figs. 4a and b, it can be seen that in this period of time, the soil is the main source of heat. Additional energy is added using the heat pump when raising the temperature level. The COPs depend on T_{soil} , they are $3.44 < 1/\eta_{30} < 7.00$ and $2.30 < 1/\eta_{45} < 3.41$, respectively. In the last days, the solar thermal panels provide only low-temperature heat at the level of $T = 15^\circ\text{C}$, on the earlier days, higher temperatures are provided. The utilisation of the storage tanks is similar for both scenarios (see Fig 4c through f), as well: In the beginning of the chosen period, the storage tanks are almost completely at the lowest possible temperature level. Until the sixth to seventh day, the storage tanks are then heated up. The next few days, the sun can fully recover the cold storage by day, but the warm storage is gradually emptied regardless of the optimisation goal. In the end of the period, both storage tanks are empty, again. Also note that the level of 45°C is occasionally used for heating. This is due to the way that auxiliary energy for pumping is considered in this specific case study. When heat is provided by the heating rod, i.e. at the 10th of February, the overall efficiency of this technology plus pumping favors the higher level. Heating efficiency is considered to be constant for the two possible levels and electricity for pumping can be saved by providing less volume at the higher temperature.

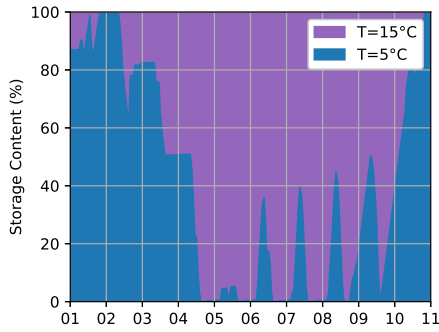
When optimising for prices or exergy, the overall trend of the heat balance is very similar. This is due to the fact that the chosen energy system design does not leave much flexibility to alter the control strategy when the other optimisation goal is followed. However, there are significant differences: In particular, in the price-optimised case, the heating rod is operated at nights, where the prices are lower. In the exergy-optimised case, it is operated by day, as the share of renewable energies tends to be higher by day, resulting in a lower exergy-rating. This difference can also be seen in the content of the warm storage, which is used to store 45°C at the last day for the price-optimal but not for the exergy-optimal case. Another difference is visible for the 2nd and 3rd day: In the exergy-optimal case, heat is preferably drawn from the cold storage,



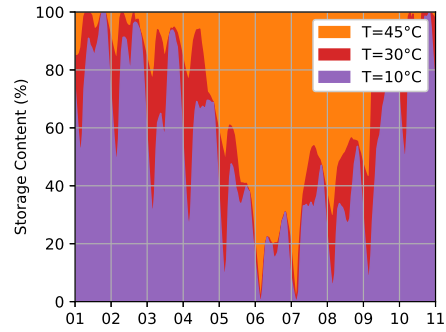
(a) Hourly heat balance in the exergy-optimised case.



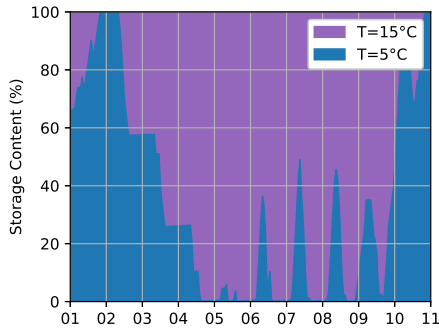
(b) Hourly heat balance in the price-optimised case.



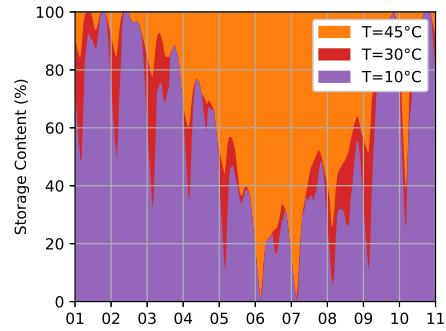
(c) Cold storage, exergy-optimised



(d) Warm storage, exergy-optimised



(e) Cold storage, price-optimised



(f) Warm storage, price-optimised

Figure 4: Hourly heat balance and storage contents for the first half of February. For a, b, the lines mark demands, the colored areas denote supply. Panels c through f indicate usage of the volume.

while the geothermal source is preferred for the price-optimal case. Considering the similarities in the temporal profiles, it is no surprise that the final value for the price or the exergy, only increases by 1%, when the other variable is optimised (see Table. 2). Over the full year, the most significant difference is seen in the operation of the solar plant. The price-optimal solution prefers the level at 45 °C more often, while the exergy-optimal one prefers 30 °C. The latter comes at the cost of a 4.7% increase of needed pumping electricity.

4 Conclusion

This paper presents a method to simultaneously optimise both, temperature and energy within energy systems, using linear programming. It uses discrete temperature levels and can work without binary or integer variables. Using the technique, an example study was conducted, showing the potential of the method.

The study optimises unit commitment, including the choice of operational temperatures, for time-dependent exergy ratings and prices. Even though the example energy system does not allow for much flexibility, differences between the two optimisation scenarios are visible. In particular, differences have been shown in the operation of the heat pump, in switching supply temperatures and in the timings for using the heating rod.

Concluding, the presented method is capable of optimising unit commitment and operation of heat supply including the choice of operational temperatures, using the well-established method of linear programming.

Author contributions

Conceptualization, methodology, validation: P.S., H.T., P.D., B.H., K.v.M., and C.A.; software, formal analysis, investigation, data curation: P.S., A.G., P.D., and B.N.; writing–original draft preparation: P.S. and A.G.; writing–review and editing: P.S., A.G., B.N., H.T., P.D., P.K. and B.H.; visualization: P.S. and A.G.; supervision: P.K. and B.H.; project administration: P.K.; funding acquisition: P.K., B.H., K.v.M., and C.A.; All authors have read and agreed to the published version of the manuscript.

Acknowledgements

This work has been funded by the Federal Ministry for Economic Affairs and Energy (BMWi) of Germany and the Federal Ministry of Education and Research (BMBF) of Germany (grant number 03SBE111).

Conflict of interest

The authors declare that they have no conflict of interest.

References

- [1] O. Lucon, D. Ürge Vorsatz, A. Zain Ahmed, H. Akbari, P. Bertoldi, L. F. Cabeza, N. Eyre, A. Gadgil, L. D., D. Harvey, Y. Jiang, E. Liphoto, S. Mirasgedis, S. Murakami, J. Parikh, C. Pyke, and M. V. Vilariño. *Buildings*, chapter 9. Volume Fifth Assessment Report of the Intergovernmental Panel on Climate Change of Edenhofer et al. [28], 2014.
- [2] Renewables 2020, 2020.
- [3] R. Franke. Object-oriented modeling of solar heating systems. *Solar Energy*, 60(3):171 – 180, 1997.
- [4] Rejane De Césaró Oliveski, Arno Krenzinger, and Horácio A. Vielmo. Comparison between models for the simulation of hot water storage tanks. *Solar Energy*, 75(2):121 – 134, 2003.
- [5] Marc A. Rosen. The exergy of stratified thermal energy storages. *Solar Energy*, 71(3):173–185, 2001.
- [6] Matteo Giacomo Prina, Giampaolo Manzolini, David Moser, Benedetto Nastasi, and Wolfram Sparber. Classification and challenges of bottom-up energy system models - a review. *Renewable and Sustainable Energy Reviews*, 129:109917, 2020.
- [7] Md. Nasimul Islam Maruf. Sector coupling in the north sea region—a review on the energy system modelling perspective. *Energies*, 12(22), 2019.
- [8] Samira Fazlollahi, Gwenaëlle Becker, and François Maréchal. Multi-objectives, multi-period optimization of district energy systems: Ii—daily thermal storage. *Computers & Chemical Engineering*, 71:648 – 662, 2014.
- [9] T. Mertz, S. Serra, A. Henon, and J.M. Reneaume. A MINLP optimization of the configuration and the design of a district heating network: Study case on an existing site. *Energy Procedia*, 116:236–248, 2017.
- [10] Shaojun Huang, Weichu Tang, Qiuwei Wu, and Canbing Li. Network constrained economic dispatch of integrated heat and electricity systems through mixed integer conic programming. *Energy*, 179:464 – 474, 2019.
- [11] Marc Hohmann, Joseph Warrington, and John Lygeros. A two-stage polynomial approach to stochastic optimization of district heating networks. *Sustainable Energy, Grids and Networks*, 17:100177, 2019.
- [12] Thomas Schütz, Rita Streblov, and Dirk Müller. A comparison of thermal energy storage models for building energy system optimization. *Energy and Buildings*, 93:23 – 31, 2015.
- [13] R. Bavière and M. Vallée. Optimal temperature control of large scale district heating networks. *Energy Procedia*, 149:69 – 78, 2018. 16th International Symposium on District Heating and Cooling, DHC2018, 9–12 September 2018, Hamburg, Germany.

- [14] Loïc Giraud, Massinissa Merabet, Roland Baviere, and Mathieu Vallée. Optimal control of district heating systems using dynamic simulation and mixed integer linear programming. In *Proceedings of the 12th International Modelica Conference, Prague, Czech Republic, May 15-17, 2017*, number 132, pages 141–150. Linköping University Electronic Press, 2017.
- [15] Ryohei Yokoyama, Hiroyuki Kitano, and Tetsuya Wakui. Optimal operation of heat supply systems with piping network. *Energy*, 137:888 – 897, 2017.
- [16] Uwe Krien, Patrik Schönfeldt, Jann Launer, Simon Hilpert, Cord Kalde-meyer, and Guido Pleßmann. oemof.solph—a model generator for linear and mixed-integer linear optimisation of energy systems. *Software Impacts*, 6:100028, 2020.
- [17] Bhawana Neupane. Exergy as assessment criterion for multimodal supply concepts in a model residential area for future energy supply. Master’s thesis, Carl von Ossietzky Universität Oldenburg, 2019.
- [18] Helen Becker and François Maréchal. Targeting industrial heat pump integration in multi-period problems. In Iftekhar A. Karimi and Rajagopalan Srinivasan, editors, *11th International Symposium on Process Systems Engineering*, volume 31 of *Computer Aided Chemical Engineering*, pages 415 – 419. Elsevier, 2012.
- [19] M. Carrion and J. M. Arroyo. A computationally efficient mixed-integer linear formulation for the thermal unit commitment problem. *IEEE Transactions on Power Systems*, 21(3):1371–1378, 2006.
- [20] Juan Alemany, Leszek Kasprzyk, and Fernando Magnago. Effects of binary variables in mixed integer linear programming based unit commitment in large-scale electricity markets. *Electric Power Systems Research*, 160:429 – 438, 2018.
- [21] <https://helleheide.de/>.
- [22] Steffen Wehkamp, Lucas Schmeling, Lena Vorspel, Fabian Roelcke, and Kai-Lukas Windmeier. District energy systems: Challenges and new tools for planning and evaluation. *Energies*, 13(11), 2020.
- [23] TU Braunschweig IGS and Steinbeis-Innovationszentrum Energie-, Gebäude- und Solartechnik energieplus. Verbundvorhaben EnStadtEs-West: Klimaneutrales Stadtquartier Neue Weststadt Esslingen, Generische Gebäudesimulation als Bestandteil der Quartier-Simulationssoftware “QuaSi”.
- [24] Noah Pflugradt and Urs Muntwyler. Synthesizing residential load profiles using behavior simulation. *Energy Procedia*, 122:655 – 660, 2017. CIS-BAT 2017 International ConferenceFuture Buildings & Districts – Energy Efficiency from Nano to Urban Scale.
- [25] Adrian Grimm. Deduction of emissions-, exergy- and price-optimised control strategies for a sector-coupled district energy system. Master’s thesis, Carl von Ossietzky Universität Oldenburg, 2020.

- [26] Entso-e Transparency Plattform.
- [27] Sachstand Primärenergiefaktoren.
- [28] O. Edenhofer, R. Pichs-Madruga, Y. Sokona, E. Farahani, S. Kadner, K. Seyboth, A. Adler, I. Baum, S. Brunner, P. Eickemeier, B. Kriemann, J. Savolainen, S. Schlömer, C. von Stechow, T. Zwickel, and J.C. Minx, editors. *Climate Change 2014: Mitigation of Climate Change*. Cambridge University Press, United Kingdom and New York, NY, USA, 2004.